REPORT DOCUMENTATION PAGE

The public reporting burden for this collection of information is estimated to average 1 hour per response, including the time for reviewing instructions, searching existing data sources, gathering end maintaining the data needed, and completing and reviewing the collection of information. Send comments regarding this burden estimate or any other aspect of this collection of information, including suggestions for reducing the burden, to the Department of Defense, Executive Service Directorate (0704-0188). Respondents should be aware thet notwithstanding any other provision of law, no person shall be subject to any penalty for failing to comply with a collection of information if it does not display a currently valid OMB control number.
PLEASE DO NOT RETURN YOUR FORM TO THE ABOVE ORGANIZATION.

1. REPORT DATE (DD-MM-YYYY) 06/23/2009	2. REPORT TYPE Final	3. DATES COVERED (From - To) 9/30/2005-12/31/2008

4. TITLE AND SUBTITLE
Computational Design of ZrO2-SiO2 Coatings for Oxidation of ZrB2/ZrC Composites
Containing ZrSix Intermetallics at 1700 degrees C

5a. CONTRACT NUMBER
FA9550-05-1-0494

5b. GRANT NUMBER

5c. PROGRAM ELEMENT NUMBER

6. AUTHOR(S)
Bronson, A and Chessa, J

5d. PROJECT NUMBER

5e. TASK NUMBER

5f. WORK UNIT NUMBER

7. PERFORMING ORGANIZATION NAME(S) AND ADDRESS(ES)
Department of Mechanical Engineering
University of Texas at El Paso

8. PERFORMING ORGANIZATION REPORT NUMBER

9. SPONSORING/MONITORING AGENCY NAME(S) AND ADDRESS(ES)
Dr. Joan Fuller
AFOSR
875 N Randolph St
Arlington VA 22203

10. SPONSOR/MONITOR'S ACRONYM(S)

11. SPONSOR/MONITOR'S REPORT NUMBER(S)

12. DISTRIBUTION/AVAILABILITY STATEMENT
Distribution A

13. SUPPLEMENTARY NOTES

14. ABSTRACT
The research group investigated specifically the microstructural phases by integrating the computational mechanics and strategic experimentation of a ZrB2/ZrC/Zr-Si composite at ultrahigh temperatures (>=1700 degrees C) in an oxidizing atmosphere. The objective of the proposed research was to study the computational aided design of ZrO2-SiO2 coatings for ZrB2/ZrC/Zr-Si composite developed by reacting B4C with Zr-Si melts through the following two integrated research thrusts:
1) Investigate the effect of microstructural design on the fundamental durability of ZrB2/ZrC/Zr-Si for use at ultrahigh temperatures
2) Investigate the processing of B4C with Zr-Si melts to create the desired scale interphase with ZrSix precipitates as determined by the numerical modeling

15. SUBJECT TERMS
Zr, Si, numerical, precipitates

16. SECURITY CLASSIFICATION OF:			17. LIMITATION OF ABSTRACT	18. NUMBER OF PAGES	19a. NAME OF RESPONSIBLE PERSON Joan Fuller
a. REPORT	b. ABSTRACT	c. THIS PAGE			19b. TELEPHONE NUMBER (Include area code) 703-696-7236

FINAL REPORT

for the

Research Project
(AFOSR Award Number – FA9550-05-1-0494)

Entitled

Computational Design of ZrO_2-SiO_2 Coatings for Oxidation of ZrB_2/ZrC
Composites Containing $ZrSi_x$ Intermetallics at 1700°C

By

Arturo Bronson and Jack Chessa
Department of Mechanical Engineering
University of Texas at El Paso

March 2009

20090630410

Executive Summary

AFOSR RESEARCH PROJECT
Computational Design of ZrO_2-SiO_2 Coatings for Oxidation of ZrB_2/ZrC Composites Containing $ZrSi_x$ Intermetallics at 1700°C

Arturo Bronson and Jack Chessa
University of Texas at El Paso

The research group investigated specifically the microstructural phases by integrating the computational mechanics and strategic experimentation of a ZrB_2/ZrC/Zr-Si composite at ultrahigh temperatures ($\geq$1700°C) in an oxidizing atmosphere. The objective of the proposed research was to study the computational-aided design of ZrO_2-SiO_2 coatings for a ZrB_2/ZrC/Zr-Si composite developed by reacting B_4C with Zr-Si melts through the following two integrated research thrusts:

- Investigate the effect of microstructural design (e.g., ZrO_2-SiO_2) on the fundamental durability of ZrB_2/ZrC/Zr-Si for use at ultrahigh temperatures (>1600°C);
- Investigate the processing of B_4C with Zr-Si melts to create the desired scale interphase with $ZrSi_x$ precipitates as determined by the numerical modeling.

The research has determined that the size of the ZrB_2 and ZrC precipitates creates a maximum strain on the substrate with the use of conventional finite element analysis, which was used to create a baseline for the enriched finite element method. The model of the Zr boride/carbide composite with a SiO_2/ZrO_2/$ZrSi_x$ scale simulates the development of the strain/stress distribution under a thermal load from 300 K to 1700 K. The computational analysis determined that the size of the SiO_2 and $ZrSi_x$ precipitates does not appreciably influence the durability of the microstructure. A simulated annealing optimization algorithm was also developed for an extended finite element program (called XMicro) with the purpose of optimizing the auto re-meshing of XMicro and thus minimizing its combinatorial selection of a composite's reinforcement architecture. After correcting for the overlapping of ZrO_2 precipitates within a matrix, XMicro determined that 1.96 μm as the optimal spacing of precipitates within a cluster and 20μm between clusters within a silica matrix of the scale interphase.

The Zr-Si melt was infiltrated into B_4C contained in a dielectric induction furnace with an oxygen potential of 10^{-31} atm (10^{-29} kPa) to create ZrC/ZrB_2/Zr-Si composites. The ZrC/ZrB_2/Zr-Si composite appear to sustain pesting upon oxidizing in air at 1700°C. However, a Zr/$ZrSi_2$/SiO_2 couple annealed at 1700°C for more than 72 hours indicates that the silicate layer protects the couple from oxidation. Hence, the infiltrated composite may develop sufficient porosity during ramping toward 1700°C to cause pesting, which can be circumvented with a fluid SiO_2 sealant. The research group has successfully merged the computational and experimental tasks toward optimizing the durability of the scale for a Zr boride/carbide composite.

For students involved in the research, Manny Gonzalez initiated his graduate study on the project and is now pursuing a doctorate at Northwestern University. Harita Petla and Elvia Renova finished their masters degree and are in the industrial sector and NASA, respectively. Sundeep Govathoti anticipates finishing his thesis while working full-time. Nischel Maheswariah and Alvaro Sandate will finish in July 2009 and in December 2009 after completing course work.

1. Introduction

The research project entails the computational analysis of the Zr-Si-O-C-B composite system with strategic experimentation to enhance the durability of a ZrO_2-$ZrSi_x$-SiO_2 scale enveloping a $ZrB_2/ZrC/Zr$-Si matrix. The scale interphase for modeling was determined by reviewing the phase equilibria according to the Zr-Si-O phase diagram at 1800°C [Peña96], as shown in Figure 1. The terminal constituents of a composition to Zr_5Si_3 and SiO_2 would correspond to the Zr metal in the matrix and silica on the outer layer of the scale, as represented

Figure 1: Zr-Si-O phase diagram developed from binary diagrams at 1800°C

by the Zr_5Si_3-SiO_2 join. The oxidation of the matrix would create primarily a SiO_2/ZrO_2 scale with the silicide emerging along the scale/matrix interface, as shown in Figure 2. The diffusional path must cross the join at least once as a result of the mass balance, which suggests that ZrO_2 would form with the silicide (i.e., Si_3Zr_5, $SiZr_2$, or Si_2Zr_3) precipitating along the ZrO_2/Zr-Si interface. The specific silicide developed along the scale/matrix interphase will depend on the

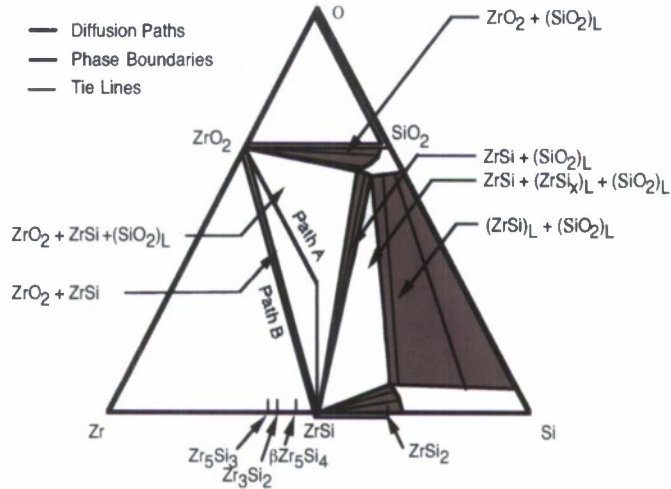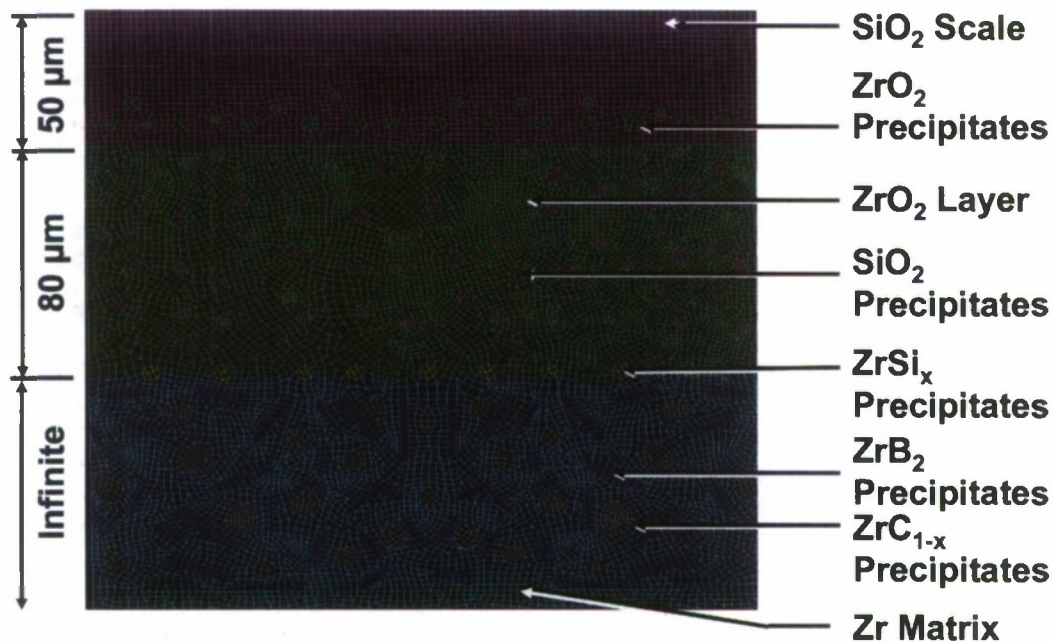Figure 2: Baseline mesh of the microstructure of ZrB2-ZrC/Zr-Si System

kinetics of the silicide reaction. Hence, the baseline mesh developed in LS-DYNA for modeling the scale/matrix region is shown in Figure 2. The $ZrSi_x$ precipitates simulate the silicide along the scale/matrix interface as a first step. For example, as the oxygen diffusional path proceeds from the silica surface inwardly, the ZrO_2 forms with a gradient of silica precipitates representative of the ZrO_2-SiO_2 phase field in the Zr-Si-O phase diagram. The silicide would develop at the ZrO_2-Zr interface as a consequence of the ternary phase field of ZrO_2-SiZr-Zr shown in Figure 1. In the following sections, the computational modeling of the research will be summarized and continued with the experimental effort in investigating the Zr-Si/B_4C reactive infiltration. After the synopsis of the research, the accomplishments and new findings of the investigation are presented.

2. Synopsis of Research

2.1 Damage modeling with LS-DYNA: The durability of the ZrB_2-ZrC/Zr-Si composite at ultrahigh temperatures was simulated with conventional finite element software of the LS-
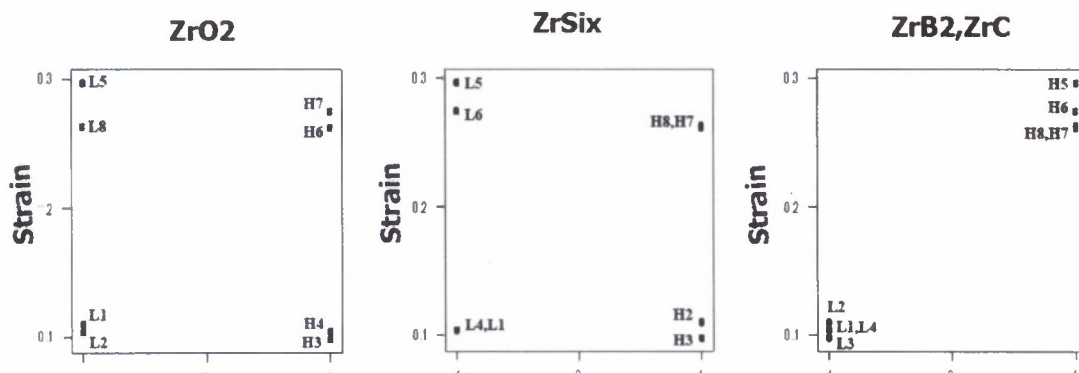

Figure 3: The effect of ZrO_2, $ZrSi_x$, ZrB_2 and ZrC on the strain simulated in Figure 2.

DYNA code developed by Livermore Software Technology Corporation (LSTC). The strain of the interphase simulation (depicted in Figure 2) was calculated via a design of experiments (DOE) factorial study. The number of simulations (N) considered the replica (R), the levels (L) of importance for high and low extremes of the effect of parameters or factors (k) consisting of ZrB_2 fibers, ZrC precipitates, ZrO_2 precipitates and $ZrSi_x$ precipitates, as summarized in equation (1).

$$N = RL^k \tag{1}$$

The simulated scale consists of duplex layers consisting of silica matrix with ZrO_2 precipitates and a zirconia matrix with SiO_2 precipitates, as depicted in Figure 2. The ZrO_2 precipitates are near the SiO_2/ZrO_2 interface while the SiO_2 precipitates are evenly distributed within the ZrO_2 matrix. The individual effects of the DOE study determined that the areas (or size) of the ZrO_2 and $ZrSi_x$ precipitates have little effect on the strain as indicated by the high and low levels for ZrO_2 and $ZrSi_x$ shown in Figure 3. However, the size of the ZrB_2 and ZrC affects the strain, as indicative of groupings at the low or high levels. The calculated strains are significantly higher
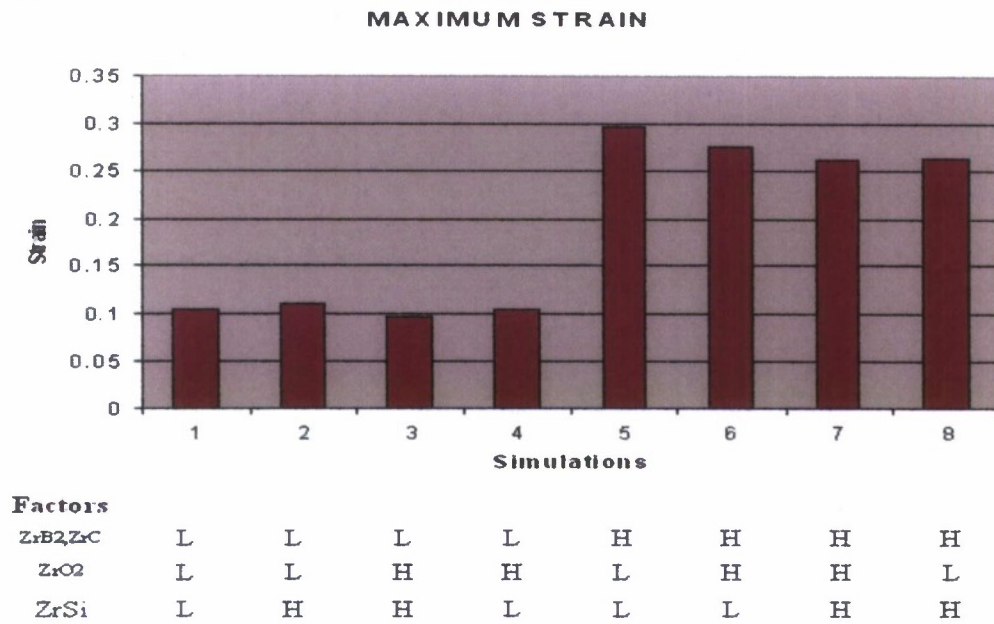
MAXIMUM STRAIN

Factors								
ZrB2ZrC	L	L	L	L	H	H	H	H
ZrO2	L	L	H	H	L	H	H	L
ZrSi	L	H	H	L	L	L	H	H

Figure 4: Calculated strain according to the design of experiments (DOE).
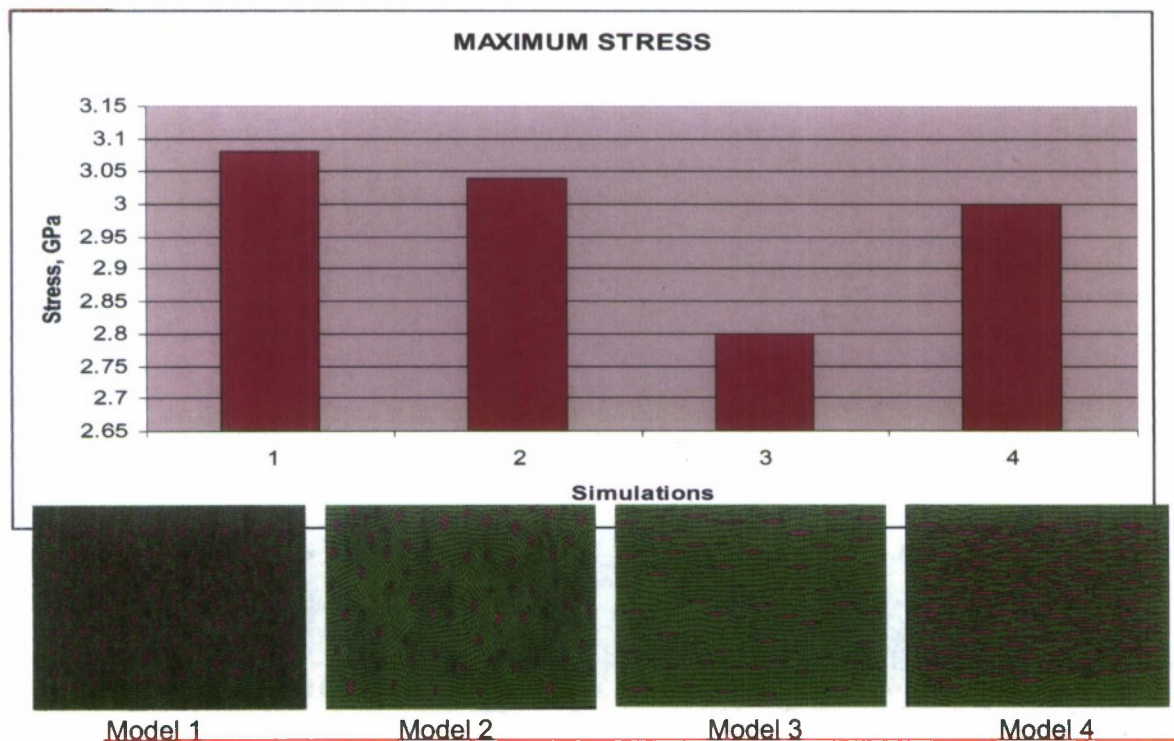
MAXIMUM STRESS

Figure 5: Calculated stress of the ZrO_2-SiO_2 layer considering the distribution of SiO_2 precipitates and their aspect ratio perpendicular or parallel with the scale/matrix interface.

for the simulations with larger areas of boride and carbide precipitates, as shown in Figure 4.

Within the ZrO_2 layer, SiO_2 precipitates simulate their development between the ZrO_2 grains or along the grain boundaries. The silica distribution within the zirconia layer were also considered by either the ratio of SiO_2 to ZrO_2 ratio or the alignment of the SiO_2 precipitates as shown in Figure 5. The SiO_2 precipitates are elongated perpendicularly to the SiO_2/ZrO_2 interface for models 1 and 2 and parallel to the interface for models 3 and 4. For the four configurations, the stress decreases from approximately 3.0 GPa to 2.8 GPa for a sparsely distributed SiO_2 precipitation elongated parallel to the SiO_2/ZrO_2 interface, as shown in Figure 5.

2.1. Oxidation model development: Oxygen diffusion was added to the XMicro code to allow for the more realistic continuum modeling of phase oxidation. In our previous studies the stress distribution was purely a result of thermal expansion mismatch as well as conventional mechanical loading. The prior phase growth law was a very crude Deal–Grove based model for which insufficient material data was even present to reasonably include into the modeling. The addition of this diffusion model and the continuum modeling of the phase oxidation allows the optimization routines to consider the effect of how precipitate location will help/hinder the oxygen transport and possibly aid as a barrier.

For example, if we consider the following oxidation
$$ZrSi + 2O_2 \rightarrow ZrO_2 + SiO_2 \tag{2}$$
The concentration evolution is governed by Fick's second law
$$\frac{d}{dx}C = \nabla.(D\nabla C) \tag{3}$$
By virtue of the level set definition of the microstructural boundaries the material value of the diffusivity, D, can be integrated exactly for each phase. At the phase interface the growth rate, or interface speed, w^{int} can be given locally from the jump in the oxygen concentration at the interface of the growth rate of the phase at the interface is given by the following reaction equation
$$w = \bar{h}\langle C \rangle \tag{4}$$
where $\langle C \rangle$ denotes the jump in the concentration at the phase interface and h is the reaction coefficient at an isoactivity of oxygen given by
$$\bar{h} = h\left(\frac{MW}{\rho}\right)_{O_2} \tag{5}$$
With the given growth rate an extensional velocity field F can be developed that will update the phase level set, ϕ by the following Hamilton-Jacobi equation [Seth99]
$$\frac{d\phi}{dx} + F|\nabla\phi| = 0 \tag{6}$$
Critical to this approach is the ability to capture the discontinuity in the concentration at the interface. This is accomplished by enriching the concentration approximation field with the Heaviside function [Ches02]. Results were presented at the Seventh World Congress of Computational Mechanics (WCCM VII).

This phase growth allows for the update of the microstructure in the fixed grid computation. We have finished some integration of the oxidation and crack models into a single code. Once the XMICRO code computes porosity along with crack models, it will be able to predict the large-

scale failure of such composites with respect to thermal mismatch and oxide growth stresses, as shown in Figure 6. Concurrent with this integration we have looked at the effect of the microstructure on the throttling of the oxygen diffusion, which will hopefully retard the phase growth stresses resulting from $ZrSi_x$ and ZrO_2 formation.
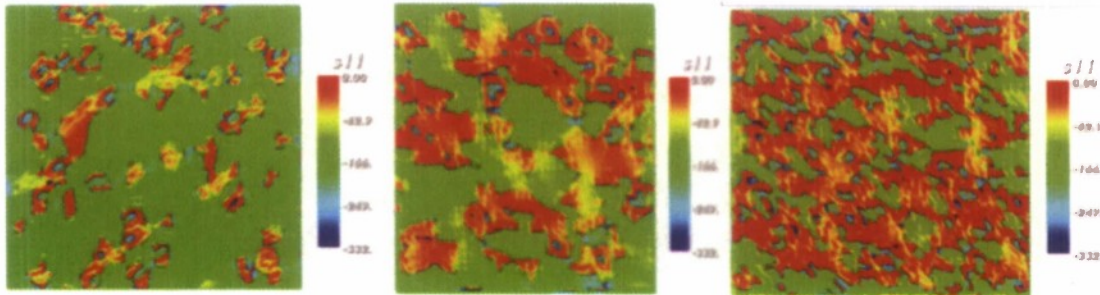

Figure 6 Example of computation of various microstructures performed on a single grid with XMICRO. Here the microstructure defining level set was generated by the GENMICRO code.

2.2. Crack growth/evolution model: As mentioned previously we have integrated the oxidation and crack models into a single code. At present the crack growth model exists in a research code for another research project. Both codes have been developed in the Computational Mechanics Laboratory and in Fortran 90 within the XMicro code to predict the large-scale failure of such composites with respect to thermal mismatch and oxide growth stresses. The methodology employed in modeling the crack growth is essentially identical to that published in Stazi et al. [Stazi03]. The important contribution is to couple the thermal growth and mismatch stresses to the crack model to predict the evolution from small-scale damage to large-scale fracture, spallation and delamination.

2.3. Reactivity of Silicides: Although the computational code for the oxygen diffusion and growth of zirconia phase is continually revised, the reactivity of the silicide phases must be probed because of the available thermodynamic data does not match the known thermodynamic phase diagram. The thermodynamic data are critical for the computational simulations because the equilibrium constants of the silicide formations are used for the backward and forward reactive steps of the overall reactions. For example, the rate (r_{ZrSi}) of ZrSi formation at steady-state is simulated according to the following expression:

$$r_{ZrSi} = k_f^{ZrSi} X_{Zr} X_{Si} - k_b^{ZrSi} X_{ZrSi} = 0 \tag{7}$$

$$K_{eq} = k_f^{ZrSi} / k_b^{ZrSi} = X_{ZrSi} / X_{Zr} X_{Si} \tag{8}$$

with the equilibrium constant (K_{eq}) representing the forward and backward rate constants (i.e., k_f^{ZrSi} and k_b^{ZrSi}, respectively).

At 1700°C, the phase diagram calculated with the available thermodynamic data [Bale02] determines the silicide compounds of ZrSi, Zr_5Si_3, and Zr_2Si, as shown in Figure 3. However, the Okamoto phase diagram [90Okam] shows that Zr_5Si_3 forms at 1745°C (2018 K) and the existence of Zr_5Si_4 and Zr_3Si_2, which are not shown in Figure 7 because of the lack of thermodynamic data. The discrepancy results from the thermodynamic inaccuracy of the data for the euctectoid temperature ($Zr_5Si_3 = Zr_3Si_2 + Zr_2Si$). The thermodynamic data for Zr_5Si_4 and Zr_3Si_2 must be incorporated into the thermodynamic modeling to determine the limits of the kinetic reactions (e.g., Equations 6 and 7).

2.4. Optimization: By virtue of the fact that the XMICRO code uses an implicit representation of the phase interfaces, a level set function, the computation for various

microstructures can be carried out on a fixed grid, as shown in Figure 3. We have developed a simple program, GENMICRO, for generating the level set functions, and therefore the microstructural geometries, from a finite set of parameters. Currently we have considered the volume fraction, aspect ratio, precipitate randomness as well as functionally grading the inclusions as parameters in a parametric study. The optimizing technique considered three simulated annealing schedules according to the following functions:
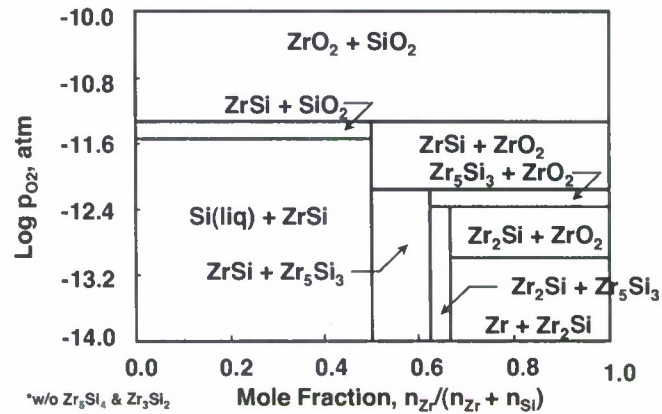

Figure 7: Calculated Zr-Si-O phase diagram from available thermodynamic data though except for Zr_5Si_4 and Zr_3Si_2.

$$T = T_0 a^{K-1} \tag{9}$$

$$T = \frac{T_0}{1+K} \tag{10}$$

$$T = \frac{T_0}{1+\ln(1+K)} \tag{11}$$

The temperature (T) depends on the initial temperature (T_0), the cooling rate (a), and the cooling cycles.

2.5. Zr-Si/B₄C Reactivity: The experimentation tested successfully the use of the graphite enclosures in the $MoSi_2$ furnace at 1700°C, but Zr-Si infiltration of B_4C was switched to the induction furnace to better sinter the B_4C packed bed. In the induction furnace, the formation of plasma hindered experimental runs even though helium was used as an inert gas to control oxidation of silicides and carbides. However, zirconium was successfully melted in the induction furnace, as an indication of reaching a temperature greater than 1855°C by decreasing the He flow rate and the temperature ramping rate.

2.6. Objectives Achieved: The research project achieved the following objectives:

1. Addition of crack and void growth
2. Addition of thermo-viscoplastic constitutive laws
3. Addition of phase growth model based on oxygen concentration gradient
4. Inclusion of topological optimization routines to automate the microstructure topological optimization. The enriched finite element methods lend themselves to topological optimization.
5. Control plasma formation during the infiltration of a Zr-Si melt into a B_4C packed bed
6. Performed oxidation of $Zr/ZrSi_2/SiO_2$ couples to determine viability of SiO_2 as an outer sealant at 1700°C.

3. Accomplishments/New Findings

3.1 Accomplishments -- In the assessment of the vaporization of SiO_2 layer formed on the $ZrB_2/ZrC/Zr$-Si composite, the research team evaluated the gaseous species at ultrahigh
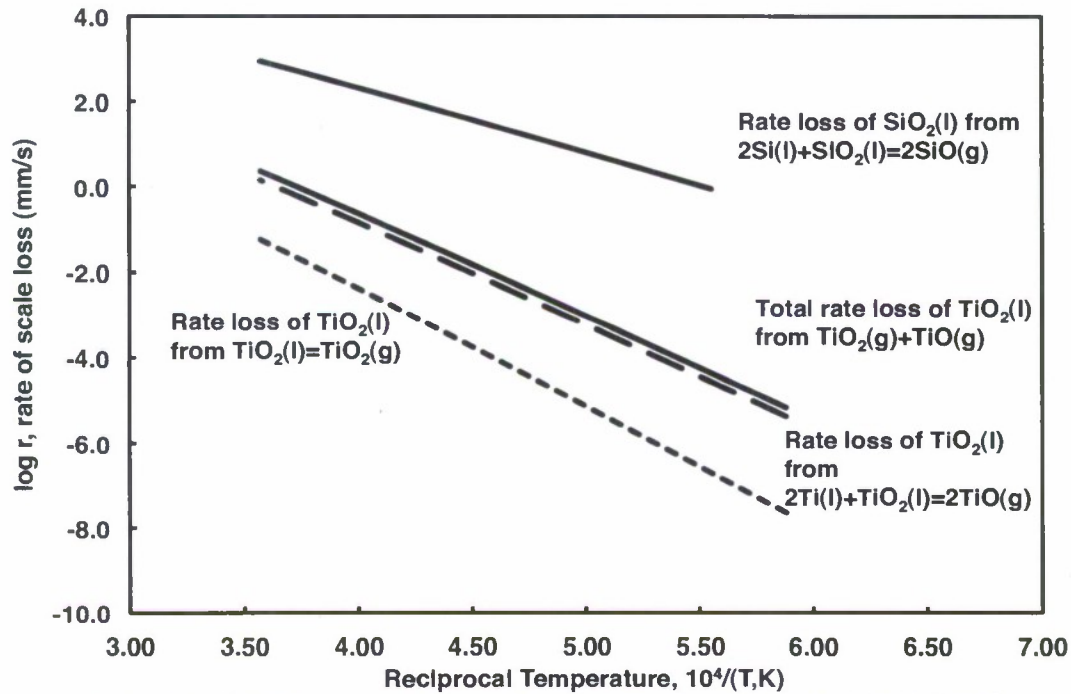

Figure 8 - The effect of the reciprocal temperature on the rate of scale loss for $SiO_2(l)$ and $TiO_2(l)$.

temperatures and the findings have been published in the Journal of the American Ceramic Society [Bron08]. For temperatures greater than 1973 K, the thermodynamic and kinetic analyses of the major gaseous species for a liquid titanate layer would vaporize significantly less than a silicate layer, when considering these layers as a protective barrier for ultrahigh temperature ceramic composites. At 2500 K, the major species is TiO(g) with $p_{TiO(g)}$= 0.1 kPa compared to SiO(g) with $p_{SiO(g)}$= $1.3(10)^3$ kPa at the Ti/TiO_2 and Si/SiO_2 equilibrium, respectively. The SiO(g) attains a partial pressure greater than ambient pressure at 2000 K even with a thermodynamic activity of 0.01 considering equilibration with a silicide (e.g., $TiSi_x$). In addition, at 2500 K the TiO_2 layer would vaporize at a rate of 0.23 mm/s compared to the SiO_2 layer's loss rate of 207 mm/s, as shown in Figure 8. Although the oxygen diffusivity and permeability through titanate solutions must be further analyzed, the thermodynamic and kinetic analyses for vaporization indicate a longer duration for a liquid titanate than for a liquid silicate layer at ultrahigh temperatures.

3.2 New Experimental Findings – The new findings experimentally consist of developing a technique for the processing of the B_4C-Zr-Si system to create a boride/carbide composite with a silicate scale and in the oxidation of the composite. In the experimentation of infiltration of Zr-Si alloys into a packed bed of B_4C, the researchers controlled the oxygen potential to less than 10^{-31} atm with a graphite enclosed system containing a Zr-Si/ZrC/ZrO_2

from 660 to 2000°C. The actual temperature reached by Zr-Si melt reacting with B_4C may reach greater than the 2200°C within the enclosure because of the exothermic reaction.

The research has determined that the size of the ZrB_2 and ZrC precipitates creates a maximum strain on the substrate with the use of conventional finite element analysis, which was used to create a baseline for the enriched finite element method. The model of the Zr boride/carbide composite with a $SiO_2/ZrO_2/ZrSi_x$ scale simulates the development of the strain/stress distribution under a thermal load from 300 K to 1700 K. The computational analysis determined that the size of the SiO_2 and $ZrSi_x$ precipitates does not appreciably influence the durability of the microstructure. The inconsequential effect of the $ZrSi_x$ precipitates on the strain distribution may result from the metal fraction amounting from 70 to 80 % within the composite containing Zr, ZrB_2 and ZrC.

Figure 9 – Induction furnace used for processing of Zr-Si melt with B_4C to create ZrB_2-ZrC-Zr-Si composite.

The Zr-Si melt infiltration into B_4C occurs in a dielectric induction furnace with an oxygen potential of 10^{-31} atm (10^{-29} kPa) to create $ZrC/ZrB_2/Zr$-Si composites, with a typical microstructure shown in Figure 2. The $ZrC/ZrB_2/Zr$-Si composite appear to sustain pesting upon oxidizing in air at 1700°C. However, a $Zr/ZrSi_2/SiO_2$ couple annealed at 1700°C for more than 72 hours indicates that the silicate layer protects the couple from oxidation. Hence, the infiltrated composite appears to develop sufficient porosity during ramping toward 1700°C to cause pesting, which can be circumvented with a fluid SiO_2 sealant.

3.3 New Computational Findings – The simulated annealing optimization algorithm was implemented to an extended finite element program (called XMicro) with the purpose of optimizing the auto re-meshing of XMicro and thus minimizing its combinatorial selection of a composite's reinforcement architecture. The mechanics of sixteen ZrO_2 precipitates ranging from 10% to 50% within a SiO_2 matrix were successfully calculated with XMicro and visualized in Paraview, as shown in Figure 11. The aspect ratio of the ZrO_2 precipitates ranged from 0.1 to 10 with their size varying from 1.8 to 90 μm within a SiO_2 domain of 900 μm.
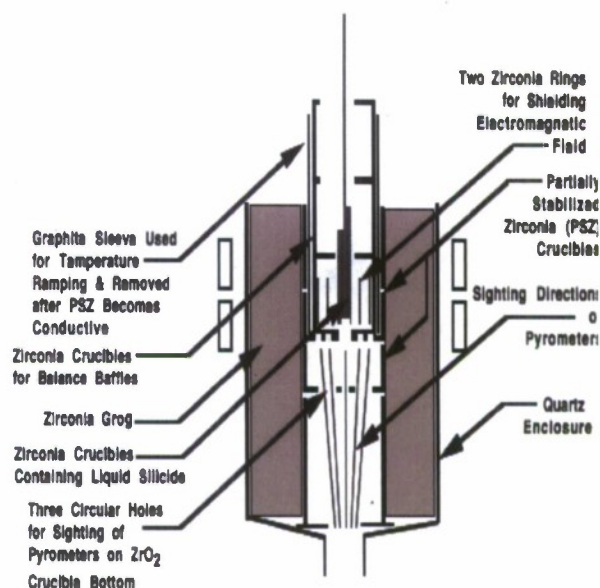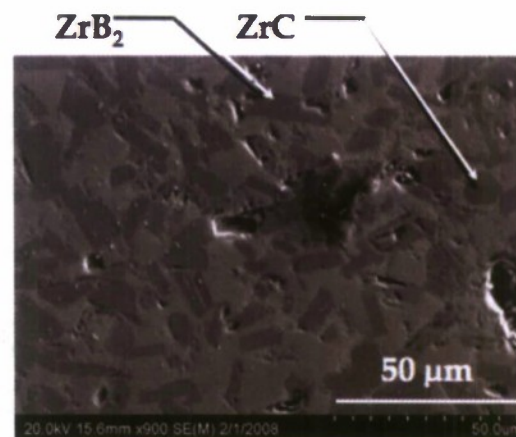

Figure 10 - Scanning electron microscope image of ZrB_2/ZrC within a Zr-Si metal phase after reacting Zr-Si with B_4C1.

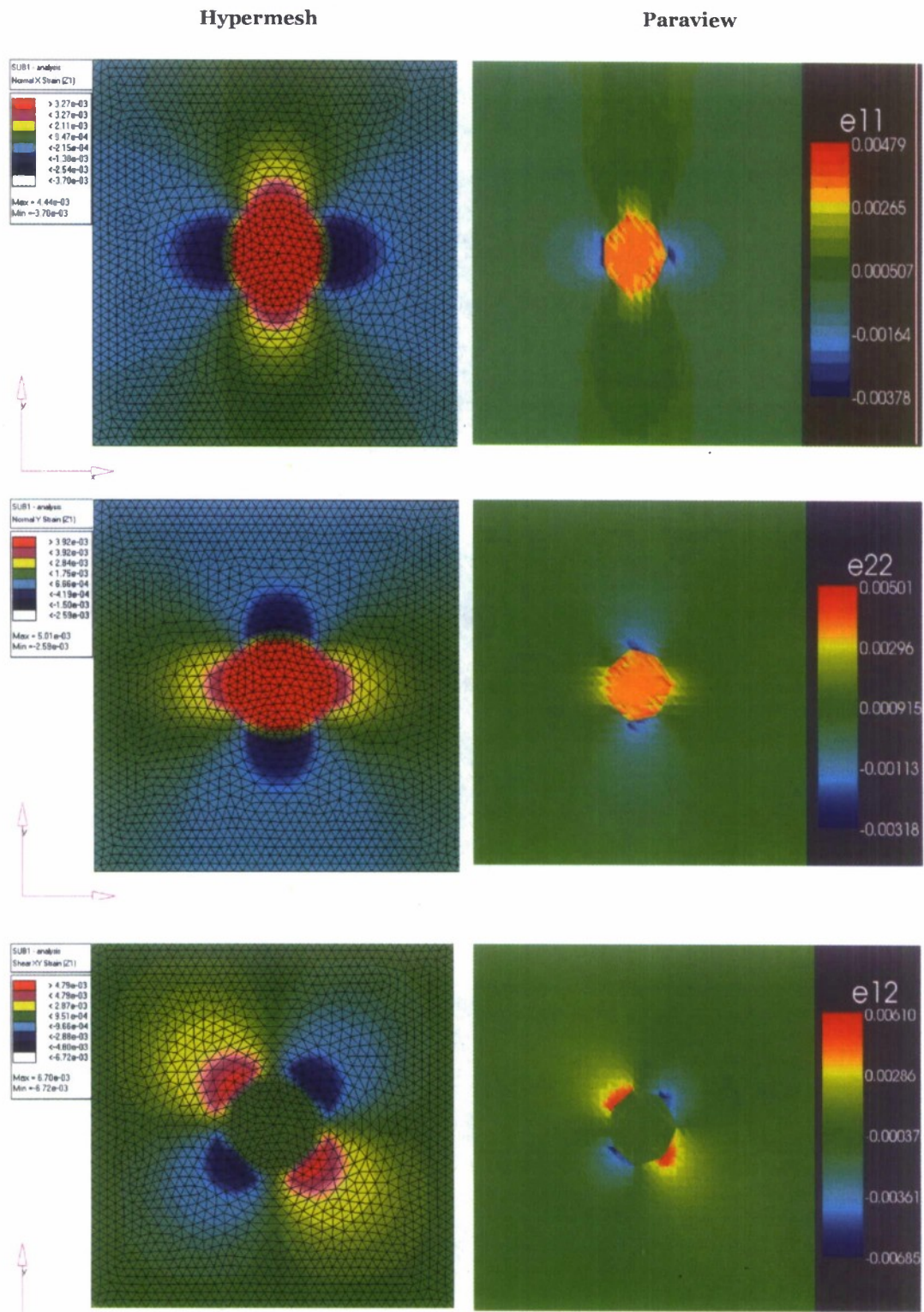**Hypermesh**   **Paraview**

Figure 11: Hypermesh compared to Paraview normal X and Y strains with shear strain contours.

After correcting the overlapping of ZrO_2 precipitates within the SiO_2 matrix, the correct variability and negligible standard deviation were acquired for sixteen precipitates with areas of 12 μm^2 and 6.8 μm^2 both creating a strain energy of 0.014 GPa/m^3. The optimal spacing of the ZrO_2 precipitates amount to 1.96 μm within a cluster and 20 μm between clusters of precipitates as shown in Figure 12.

3.4 Relevance to Air Force Mission -- The thermodynamic and kinetic analysis of the vaporization of SiO_2 and TiO_2 coatings on ceramic composites coincides with the Air Force's mission of providing ceramics and ceramic composites for future hypersonic aircraft which can attain temperatures greater than 1600°C. The computational design of the $ZrB_2/ZrC/Zr$-Si system investigates the fundamental durability at 1700°C through multiscale modeling to enable us to predict the ultrahigh temperature behavior. With the computational design of ceramic composites, scale mechanics and its oxidation can be transferred to similar systems (e.g., Zr-Ti/ZrC-ZrB_2, Hf-Ti/HfC-HfB_2 and Zr-Ti-Ta/ZrC-ZrB_2) exposed to more extreme ultrahigh temperatures.

Figure 12: Optimal calculated configuration of zirconia precipitates within a silica matrix.

4. Personnel Supported

Harita Petla, in the Department of Mechanical Engineering, finished her masters degree with a thesis [Petl08] on modeling UHTCC microstructures with standard finite element methods. Elvia Renova also finished her thesis [Reno08] with the extended finite element analysis of a composite and she has an engineering position at NASA-Huntsville. Sundeep Govathoti, a Masters Student in the Department of Mechanical Engineering, has been establishing the experimental apparatus for processing ceramic composites through Zr-Si/B_4C reactive infiltration and anticipates finishing his thesis while working full-time. Nischel Maheswariah and Alvaro Sandate continue with the processing of the Zr-Si/B_4C composite with varying Zr/Si ratio to acquire the Zr_5Si_3 and Zr_2Si, which melt incongruently at 2183 and 1925°C, respectively. Nischel anticipates finishing in July 2009 and Alvaro in December 2009 after completing course work. Nischel and Sundeep are also oxidizing a $Zr/ZrSi_2$ samples encased in a SiO_2 shell or layer to determine the extent of the silica sealant's capability to protect the silicide from oxidation. Manny Gonzalez who was previously supported on the AFOSR research project is now pursuing a doctorate in mechanical engineering at Northwestern University.

5. Publications/Interactions

A manuscript entitled, "An Analysis of the Vaporization of SiO_2 and TiO_2 from Ultrahigh Temperature Ceramic Composites," was published in the Journal of the American Ceramic Society. In addition, a presentation of the on-going research was made by Dr. Jack Chessa at the
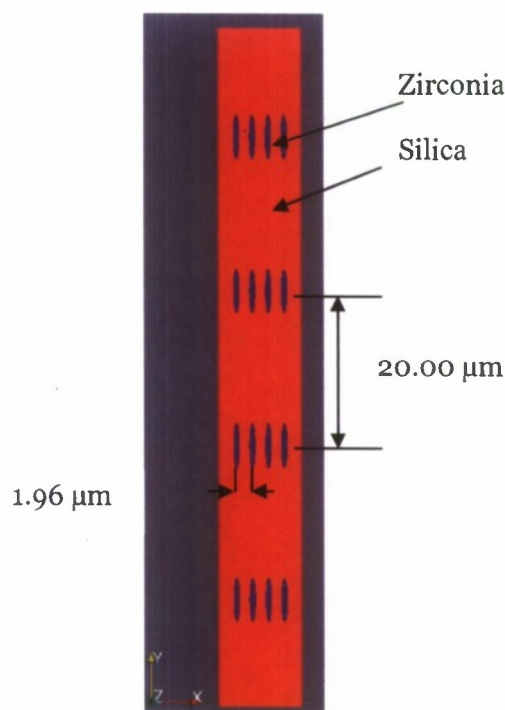
AFOSR sponsored Workshop on Ultrahigh Temperature Ceramic Materials (23-25 July 2007) at SRI International in Menlo Park, CA. He also made presentations at the 2006 FEMTEC conference in December at The University of Texas at El Paso and Seventh World Congress of Computational Mechanics (WCCM VII) in Los Angeles.

6. Patent Disclosures/Awards

No patent disclosures have been submitted, yet, though we are preparing the patent for the processing of the reactive metals to control the oxygen potential. Dr. Jack Chessa with Dr. Cesar Carrasco of the University of Texas at El Paso (UTEP) is involved in a major computational mechanics effort with Lockheed-Martin. In addition, Professor Arturo Bronson and Dr. Jack Chessa have been awarded a project by the Air Force Wright Laboratories to investigate the impact of ceramic composites at 1700°C.

7. References

Bale02   C. W. Bale, P. Chartrand, S. A. Degterov, G. Eriksson, K. Hack, R. Ben Mahfoud, J. Melançon, A. D. Pelton and S. Petersen, Calphad, 26 [2] 189-228 (2002). FactSage Thermochemical Software and Databases.

Bron08   A. Bronson and J. F. Chessa: Journal of the American Ceramic Society, 2008, Vol. 91, pp. 1448-1452. An evaluation of vaporizing rates of SiO_2 and TiO_2 as protective coatings for ultrahigh temperature ceramic composites.

Ches02   J. Chessa, P. Smolinski, and T. Belytschko. *The extended finite element method (XFEM) for solidification problems.* International Journal of Numerical Methods in Engineering, 53:1959–1977, 2002.

Okam90   H. Okamoto: Bull. Alloy Phase Diagrams, 11:513-519, 1990.

Peña96   M. Peña, C. Ramos, A. Bronson: Metallurgical Transactions B, 1996, Vol. 27B, pp. 271-276. Phase Relations of a Silicide/Silica Reaction Couple at 2273K.

Petl08   H. Petla: Computational Design of Ultra-High Temperature Ceramic Composite Materials, Masters Thesis, University of Texas at El Paso, 2008.

Reno08   E. P. Renova: Optimization of Particulate Composite Structures Analyzed by X-FEM, Masters Thesis, University of Texas at El Paso, 2008.

Seth99   J. A. Sethian. *Level set methods and fast marching methods.* Cambridge University Press, 1999.

Stazi03   F. Stazi, E. Budyn, J. Chessa, and T. Belytschko. *An extended finite element method with higher-order elements for crack problems with curvature.* Computational Mechanics, 31(1-2):38–48, 2003.

Neat SWNT Fibers and Discrete Conductors

Matteo Pasquali, Principal Investigator
Rice University

Accomplishments

Abstract

Dispersing SWNTs into superacids and spinning fibers from the resulting liquid crystalline solution is a promising and scalable way of producing neat SWNT fibers. Fuming sulfuric acid and chlorosulfonic acid were identified as good solvents for SWNTs which are otherwise extremely difficult to disperse and process at high concentrations. Chlorosulfonic acid was found to be capable of dispersing SWNTs as individuals at 17wt% concentration. In this project, different fiber spinning techniques and coagulation methods were investigated, including wet coagulation, dry coagulation and dry-jet wet-spinning. Suitable coagulants were identified for the wet-spinning of SWNT dopes and a co-flow design was successfully developed to prevent wrinkling of CNT fiber during coagulation. Extensive studies on coagulated fiber morphology suggested that slow acid removal is key to producing fewer voids. Better SWNT coalescence and alignment was obtained by using appropriate coagulant and dope concentration. Finally, we showed that chlorosulfonic acid can disperse long (50 – 500 µm) CNTs; this has important implications for producing CNT fibers that are stronger and more conductive in the near future.

Table 1 Summary of accomplishments

		Key findings/ Accomplishments
1. CNT dispersion		Successful dispersion of long (500 µm) SWNTs or MWNTs
		Successful dispersion of SWNT at high concentration (17wt%)
2. Fiber Spinning and Coagulation	Wet coagulation	*SWNT/chlorosulfonic acid dope:* A number of coagulants were identified, including chloroform, dichloromethane and diethyl-ether and 96% sulfuric acid. Co-flow apparatus was developed to successfully avoid the wrinkling in coagulated fibers
		SWNT/sulfuric acid dope: Good fiber coalescence morphology was obtained for 103% and 108% sulfuric acid. A mixture of polyvinyl alochol (<1%) and water showed better coalescence of SWNT ropes compared with using water only
	Dry coagulation	Good fiber morphology was obtained by evaporating sulfuric acid inside a vacuum oven
	Dry-jet wet spinning	Successful extrusion of SWNT/superacid under tension resulted in a tenfold improvement in fiber tensile strength

1. Carbon Nanotube (CNT) Dispersion

Successful dispersion of long (>50μm, up to 500μm) CNT in chlorosulfonic acid
Over past years, our group has shown the ability to disperse HiPco[*] single-walled carbon nanotubes (SWNTs) and other "short" (<10 μm) SWNTs in superacids such as fuming sulfuric acid and chlorosulfonic acid. Up to recently, it was commonly believed that no fluid could solubilize long (50-500 μm) SWNTs or MWNTs. However, we showed that CNTs up to 500 μm can indeed be successfully dispersed in chlorosulfonic acid as long as the CNTs are relatively defect free in their outer sidewalls. This discovery is critical for fiber-spinning since tensile strength should scale linearly with the length of the constituent nanotubes. Fibers spun from long, carpet-grown CNTs are likely to show orders of magnitude improvements in mechanical properties. Fibers spun from long CNTs are also likely to see significant improvements in conductivity.
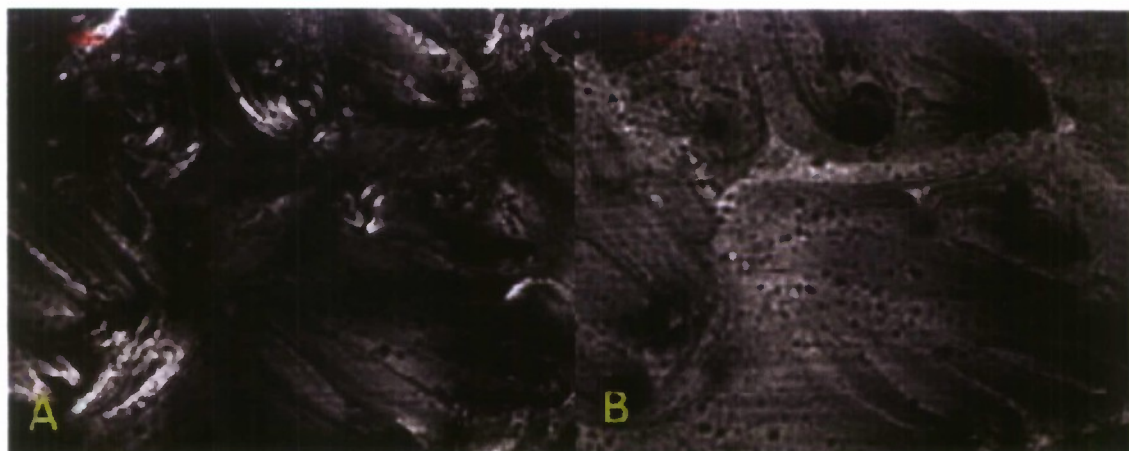

Fig. 1 Microscopy of 500 μm long carpet-grown SWNTs in chlorosulfonic acid. (A) Birefringent liquid crystalline domains under cross polarizers. (B) The same image is shown under transmitted light. Scale bars are 200 μm.

Successful dispersion of SWNT at high concentrations
Chlorosulfonic acid is a stronger acid and better solvent than oleum (120% fuming sulfuric acid). Different concentration of SWNTs (7, 10, and 12 wt%) in chlorosulfonic acid were prepared and all dispersions showed remarkable liquid crystalline behavior (Fig.2). SWNT chlorosulfonic dope with a concentration as high as 17wt% has been successfully prepared. Also, cryo-TEM evidence (Fig. 3, experiments done in collaboration with the group of Ishi Talmon and Yachin Cohen) showed that both long and short SWNTs in chlorosulfonic acid were dispersed as individuals, confirming that SWNTs form true thermodynamic molecular solutions in these superacids. (This study constitutes the first-ever cryo-TEM imaging of any superacid system.)

---

[*] HiPco: high pressure disproportionation of carbon monoxide

Fig. 2 Polarized microscopy on liquid crystalline texture in the SWNT chlorosulfonic dope: A) 7 wt%, B) 10 wt%, C) 12 wt% SWNT.
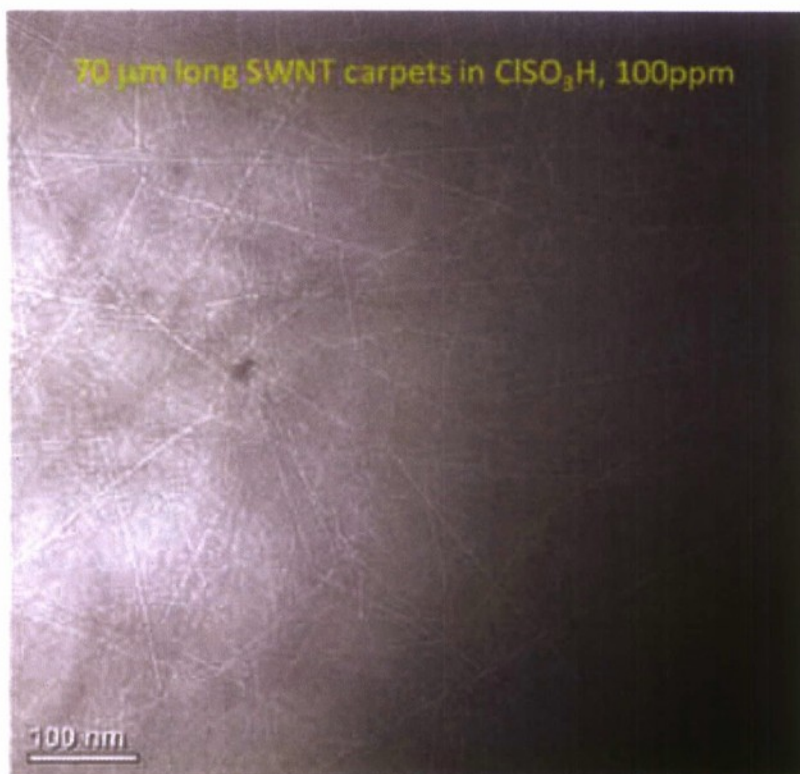

Fig. 3 Cryo-TEM images of 70μm long SWNT carpets dispersed as individuals in chlorosulfonic acid.

Fibers were spun into dichloromethane from SWNT chlorosulfonic dopes shown in Fig. 2. From SEM images, it is clear that the concentration of the dope has a direct effect on the microstructure of the final fiber (Fig. 4); as the concentration of the dope increases, the morphology of the fiber becomes smoother and more aligned.
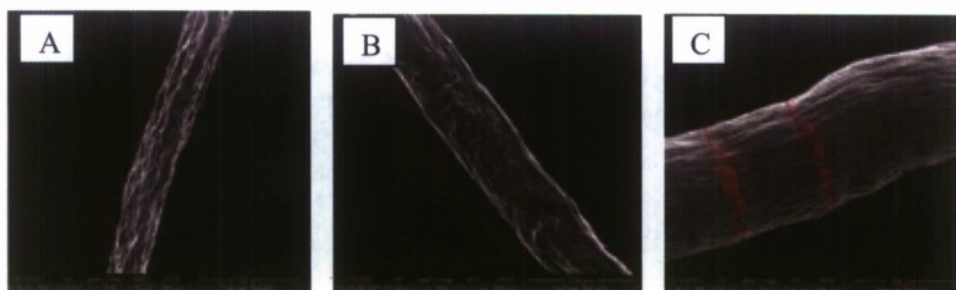
Fig. 4 Fiber microstructure as a function of SWNT concentration of dichloromethane coagulated fibers: A) 7 wt%, B) 10 wt and C) 12 wt% chlorosulfonic dope.

Until recently, it was not possible to measure rheological properties of solutions of SWNTs in chlorosulfonic acid ($ClSO_3H$) because of the difficulties of working with $ClSO_3H$. We designed and perfected a unique moisture-free rheometer setup that is ideal for studying such dispersions. This setup has yielded important data on the viscoelasticity and liquid crystallinity of such solutions.

2. Fiber-spinning and Coagulation
Wet coagulation of SWNT/chlorosulfonic acid dope

Wet-spinning is carried out by extruding the liquid crystalline SWNT/superacid solution into a coagulant bath. In order to use this technique, a series of coagulants compatible with chlorosulfonic acid has been identified. These are chloroform, dichloromethane, diethyl-ether and 96% sulfuric acid. In preliminary testing, 96% sulfuric acid was identified as a good candidate as a coagulant for chlorosulfonic dope. A direct spinning of the dope into this coagulant gave a highly irregular surface, and subsequent investigation suggested that the wrinkling was due to compressional viscous stresses. To avoid wrinkling, a co-flow apparatus has been designed that applies tension while coagulating the fiber. This eliminates surface wrinkling (Fig. 4). The smooth morphology of the co-flowed fiber shows the importance of the applied tension during the coagulation process.
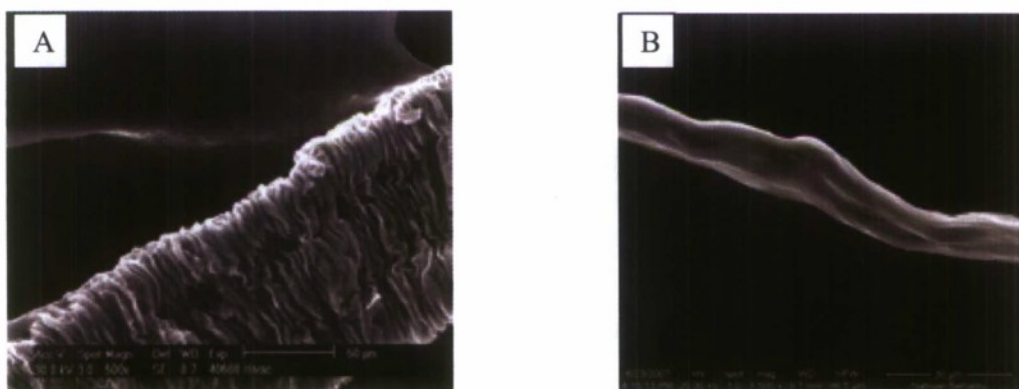

Fig. 5. Difference in microstructure of fibers coagulated in 96% Sulfuric acid: A) direct spinning (single stream), B) co-flowed.

4

Wet coagulation of SWNT/sulfuric acid dope

Previous studies of spinning of SWNTs from sulfuric acid had not explored the combination of acid strength, interaction with coagulant, and fiber structure. We tested the spinning and coagulation of SWNT fibers from various acid concentrations, keeping constant SWNT concentration. A water coagulation bath was used. As shown in Fig. 6, the morphology of the fiber varies with the superacid strength. We attribute this structural improvement to two separate effects: In weaker solvents, the acid is removed more slowly, which yields better coalescence of the SWNT into larger structures with few voids. However, stronger solvents disperse the SWNTs more effectively, resulting in better alignment. Figure 6 shows a comparison between 120%, 108%, 103%, and <100% illustrating the poor coalescence morphology at the extremes (120% and <100%) and the better coalescence between 103% and 108%. The poor morphology below 100% acid is due to loss of liquid crystalline behavior in the dope and formation of a crystal solvate (alewives).
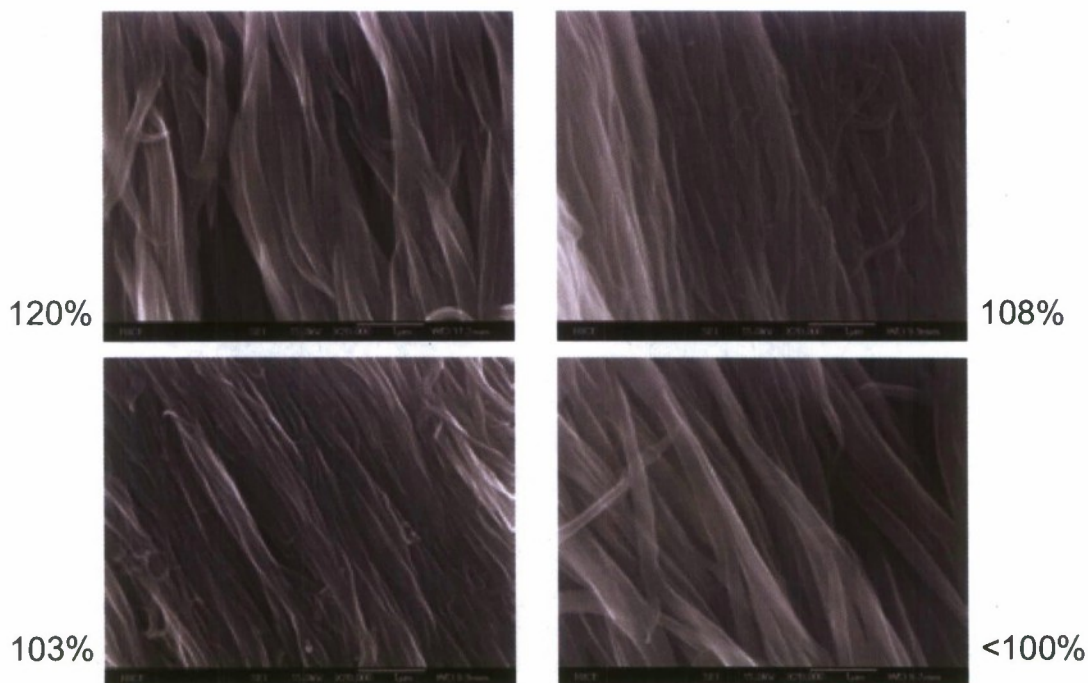

Fig. 6 SEM morphology of 8wt % SWNT with varying concentrations of sulfuric acid. At 120% and <100%, the SWNT ropes do not coalesce and there are voids, whereas in 108% and 103%, the ropes coalesce.

As shown in Fig. 7, changing the coagulant bath changed the fiber's morphology. A low weight percent (<1%) of polyvinyl alcohol (PVA) and water continues to provide the best coagulant (for fuming sulfuric acid dopes) by coating the fiber slowing down the acid removal allowing time for coalescence. The SEM image on the left shows better coalescence of SWNT ropes compared to the water only coagulant on the right. Note that water-based coagulants cannot be used for SWNT/chlorosulfonic acid dopes.
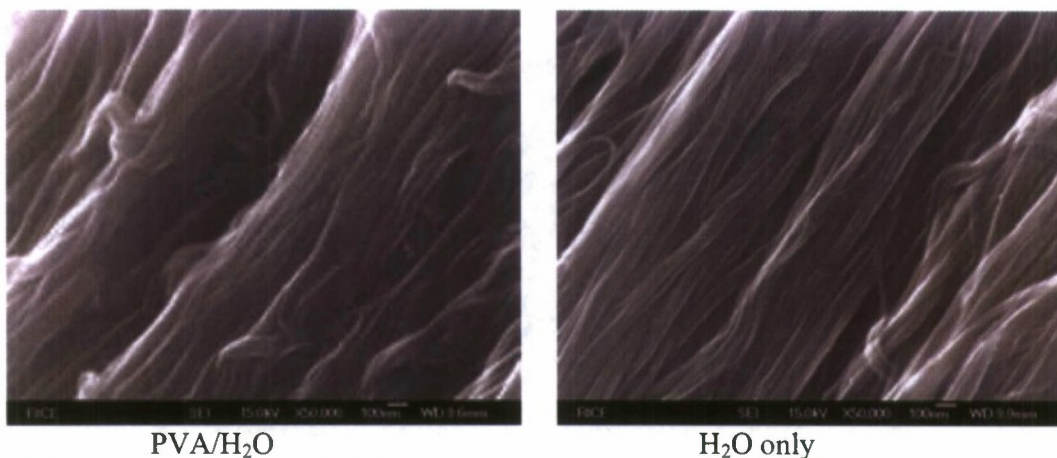
5

PVA/H$_2$O   H$_2$O only

Fig. 7 Comparison between PVA/H$_2$O and water-only coagulant on fiber morphology.

Dry coagulation

Instead of the wet coagulation process described above, SWNT dope was extruded onto Teflon tape, metal, and glass substrates and allowed to evaporate in a vacuum oven to slowly rcmove the sulfuric acid. In Fig. 8, the bottom portion of the dope that was slowly evaporated (left) is compared with the fiber is rapidly coagulated into water (right). Dry coagulation shows a smooth morphology due to the slow removal of acid; however, wet coagulation methods are scalable, so we aim to achieve a similarly slow removal of acid in the coagulation process.
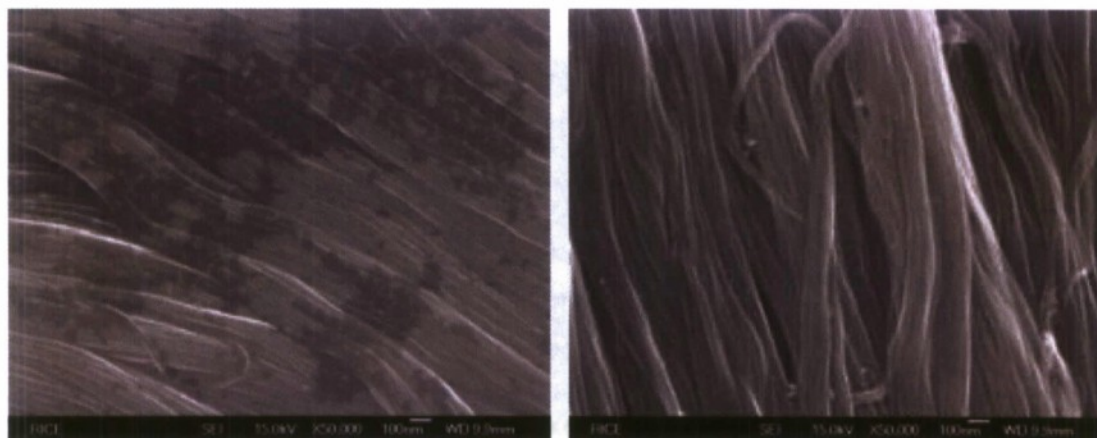
Bottom of film extruded onto metal drum.   Fiber spun from 8% SWNT in 108% sulfuric acid.

Fig. 8 Comparison between extruding dope onto a metal substrate (left) and into water (right).

Dry-jet wet spinning

After developing critical pre-processing treatments, our group successfully mixed viscous SWNT/superacid dopes capable of extrusion under tension. These dopes were extruded, drawn in air gap (Fig. 9), and coagulated in ice water to form neat SWNT fibers. The

combination of pre-processing and drawing shows a tenfold improvement in fiber tensile strength.
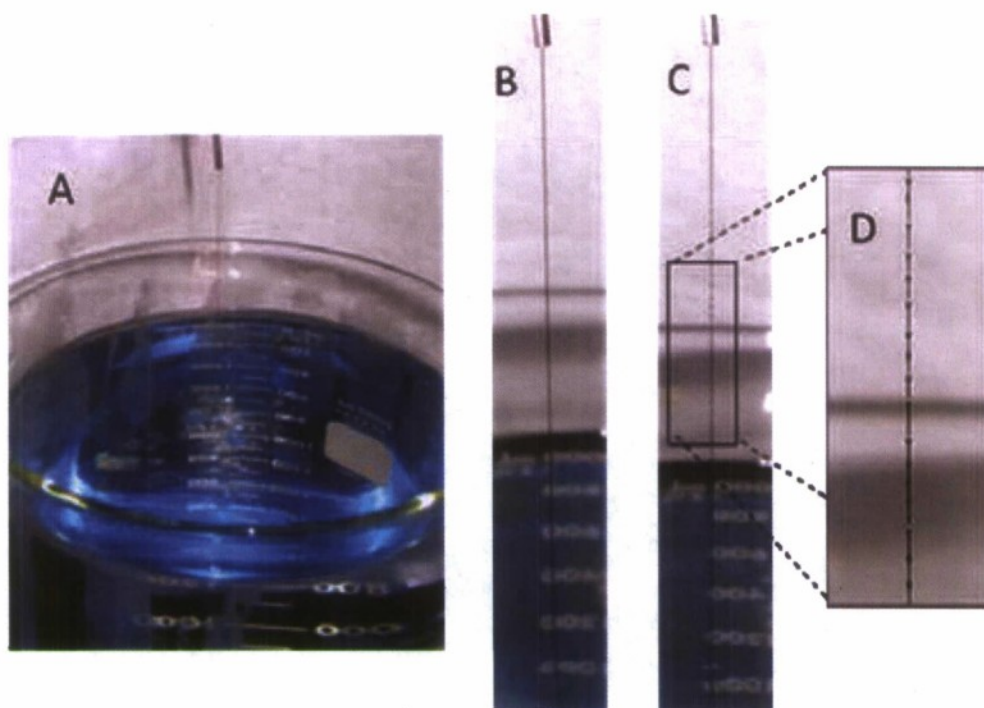

Fig. 9: SWNT dope air-gap in fiber-spinning with acidic droplets created on the surface of the newly-forming fibcr.

Other accomplishments and interactions

Collaboration with other synergistic efforts: we have collaborated with Prof James Tour on studies of ultra-short SWNTs (US-SWNTs) for composite materials (program supported by AFOSR). Within this study, we have shown that pure US-SWNTs form liquid crystalline phases that can be spun directly. The potential of these pure phases of US-SWNTs is being assessed. Fibers produced within this program area have also been evaluated by Tour for support for Hydrogen storage (under DOE funding), and as starting material for impregnation with PAN (under joint AFRL funding to Pasquali and Tour). Pasquali, Tour, Hwang, and the students involved in this AFOSR program interacted routinely with AFRL personnel Dr. Karla Strong and Dr. Benji Maruyama and collaborate with other group members working on a Rice-AFRL sponsored research on nanotailored carbon fibers. Recent developments include interactions with researchers at DuPont and Teijin Aramids and discussions of potential future collaborations in transitioning this technology to industry.

7

Program Statistics – AQW, Rice University

PI: Dr. Matteo Pasquali

Graduate Students supported by this grant: Hua Fan, Richard D. Booker; A. Nicholas G. Parra-Vasquez; Natnael Behabtu, Colin C. Young, B. Dan, Cary Pint, Dmitri E. Tsentalovich

(1) Number of PI and Co-PI involved in the research project : __1___

(2) Number of Post Doc Supported under AFOSR: __none___Dr. Micah Green (PhD MIT 2007) also works in the group. He is funded on a personal fellowship; his work benefits this AFOSR grant.

(3) Number of graduate students supported by AFOSR: __8___

(4) Other researchers supported by AFOSR: Dr. Robert Hauge, Dr. Howard Schmidt, Dr. Wen-Fang Hwang_

(5) Number of publications by PI's in the last 12 months period in refereed journals: 20 (includes 2 in press) plus 9 under review.

(6) Publications (in refereed journals only) and theses that acknowledge AFOSR supports: ___7 published plus 5 under review

Publications:

A. Parra-Vasquez, A.N.G., Behabtu, N., Green, M.J., Pasquali, M., "Chlorosulfonic acid: The ultimate nanotube solvent," *J. Am. Chem. Soc.* (2009, in preparation)

B. Green, M.J., Behabtu, N., Pasquali, M., Adams, W.W., "Nanotubes as Polymers." *Polymer* (2009, submitted)

C. Green, M.J., Parra-Vasquez, A.N.G., Behabtu, N., Pasquali, M. "Modeling the phase behavior of polydisperse rigid rods in attractive solvents, with applications to SWNTs in superacids." *J. Chem. Phys.* (2009, under review)

D. Davis, V.A., Parra-Vasquez, A.N.G., Green, M.J., Rai, P.K., Behabtu, N., Prieto, V., Booker, R.D., Schmidt, J., Kesselman, E., Zhou, W., Fan, H., Hauge, R.H., Fischer, J.E., Cohen, Y., Talmon, Y., Smalley, R.E., Pasquali, M. "Is it possible to dissolve Single-Walled Carbon Nanotubes in liquids and assemble them into macroscopically-ordered materials?" *Nature Nano* (2009, under review)

E. Booker, R.D., Green, M.J., Fan, H., Parra-Vasquez, A.N.G., Behabtu, N., Young, C.C., Schmidt, H.K., Smalley, R.E., Hwang, W.-F., Pasquali, M. "High-shear treatment of SWNT/superacid solutions as a pre-processing technique for assembly of fibers and films," *J. Nanoeng. Nanosys.,* special issue on carbon nanotubes (2009, under review)

F. B. Dan, G. Irvin, and M. Pasquali, Continuous and Scalable Fabrication of Transparent Conducting Carbon Nanotube Films. *ACS Nano*, **3**, 835-843, 2009.

G. C. L. Pint, N. Nicholas, J. G. Duque, A. N. G. Parra-Vasquez, M. Pasquali, and R. H. Hauge, Recycling ultra-thin catalyst layers for multiple single-walled carbon nanotube array regrowth cycles and selectivity in catalyst activation. *Chem. Mater.*, **21**, 1550-1556, 2009.

H. Leonard, A.D., Hudson, J.L., Fan, H., Booker, R.D., Simpson, L.J., O'Neill, K.J., Parilla, P.A., Heben, M.J., Pasquali, M., Kittrell, C., Tour, J.M., "Nanoengineered Carbon Scaffolds for Hydrogen Storage." *J. Am. Chem. Soc.* 131 (2), 723-728 (2009).

I. C. L. Pint, Y.Q. Xu, M. Pasquali, and R. H. Hauge, Formation of highly dense aligned ribbons and transparent films of single-walled carbon nanotubes directly from carpets. *ACS Nano*, **2**, 1871–1878, (2008).

J. Behabtu, N., Green, M.J., Pasquali, M. "Carbon Nanotube-based Neat Fibers." *Nano Today* 3 (5-6), 24-34 (2008, cover article).

K. C. L. Pint, S. T. Pheasant, M. Pasquali, K. Coulter, H. K. Schmidt, and R. H. Hauge, Synthesis of high aspect-ratio carbon nanotube "flying carpets" from nanostructured flake substrates. *Nano Lett.*, **8**, 1879-1883 (2008).

L. C. L. Pint, N. Nicholas, S. T. Pheasant, J. G. Duque, A. N. G. Parra-Vasquez, G. Eres, M. Pasquali, and Robert Hauge, Temperature and gas pressure effects in vertically aligned carbon nanotube growth from Fe-Mo catalyst. *J. Phys. Chem. C*, **112**, 14041–14051, (2008).

Theses:

H. Fan, Ph.D. thesis, Rice University, 2007

A. G. N. Parra-Vasquez, Ph.D. thesis, Rice University, 2009 (expected)

B. Dan, Ph.D. thesis, Rice University, 2010 (expected)

N. Behabtu, Ph.D. thesis, Rice University, 2011 (expected)

C. Pint, Ph.D. thesis, Rice University, 2011 (expected)

(7) Awards and Honors received by the Pl (life-time received):

- NSF-CAREER award (2001)
- Rice University Faculty Teaching & Mentoring Award (2009)